

Quantum pumping in graphene in the quantum Hall regime

Rakesh P. Tiwari and M. Blaauboer

Kavli Institute of Nanoscience, Delft University of Technology, Lorentzweg 1, 2628 CJ Delft, The Netherlands
(Dated: March 4, 2019)

We consider quantum pumping of Dirac fermions in a monolayer of graphene in the presence of a perpendicular magnetic field in the central pumping region. The two external pump parameters are electrical voltages applied to the graphene sheet on either side of the pumping region. We analyze this pump within scattering matrix formalism and calculate both pumped charge and spin currents. The predicted charge currents are of the order of 100 nA, which is readily observable using current technology.

PACS numbers: 72.80.Vp, 73.23.-b, 73.63.-b, 73.63.Rt

By periodically changing the confining potential of a quantum system, quantum pumping allows a net dc current of carriers to flow in the absence of an applied bias [1–3]. The possibility of generating electrical currents in solid-state nanostructures using this phenomenon has attracted considerable attention [4]. The same phenomenon allows us to adiabatically generate spin-polarized currents in solid-state nanostructures [5], which is of great interest in the field of spintronics. Usually the pumped currents are small (~ 100 pA) and difficult to identify, as such a small signal may be obscured by rectification. Indeed, quantum pumps realized so far are commonly believed to have demonstrated rectified currents [6–8]. The exceptionally high mobility of carriers (> 1 m²/Vs [9]) in graphene, a monolayer of carbon atoms arranged in a honeycomb lattice, makes it a prominent nanomaterial for generating large pumped currents. In this letter we propose a quantum pump realized in graphene in the quantum Hall regime. We predict large pumped currents (~ 100 nA) at modest values of gate voltages and magnetic fields, which increases the hope for unambiguous demonstration of quantum pumping.

Ever since the synthesis of high-quality graphene [10], there has been tremendous interest in the properties of this single-layer form of carbon [11]. Graphene has a honeycomb lattice structure, with two atoms per primitive cell and a hexagonal Brillouin zone. The Fermi energy E_F of homogeneous, neutral graphene lies at the so-called Dirac point, which occurs at high symmetry points \mathbf{K} in the Brillouin zone. In fact, there are two inequivalent Dirac points \mathbf{K}_0 and \mathbf{K}'_0 with two distinct valleys of excitations. Near the Dirac point, the density of states is linear in $|E - E_F|$ and the spectrum of quasiparticle states is well described by the Dirac equation for massless fermions. Partly as a result of this electronic structure [9, 10, 12, 13], graphene exhibits many unusual electronic and magnetic transport properties, such as a unique type of quantum Hall effect [14, 15], ballistic conduction by massless Dirac fermions [14, 15], a size-dependent band gap [16] and large magnetoresistance [13, 17–19]. Recently some quantum pumps based on graphene were proposed. Zhu and Chen [20] considered a monolayer

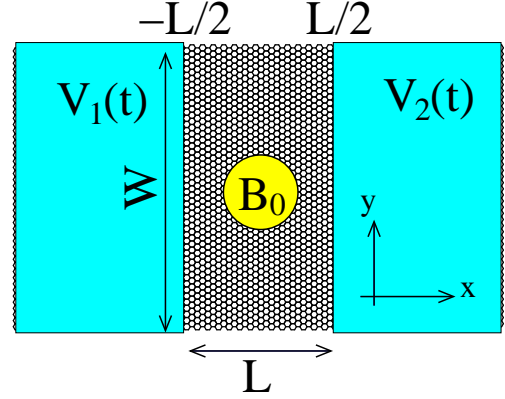


FIG. 1. (color online). Schematic of the proposed quantum pump. An external field $B_0\hat{z}$ is applied in the central pumping region. The gate voltages $V_1(t)$ and $V_2(t)$ are the two pumping parameters.

charge pump with two gate voltages as pumping parameters. Prada *et al.* [21] considered a similar charge pump and found that the current is pumped through evanescent modes in the pumping region. In our proposed set-up, both charge and spin currents are pumped through traveling modes and the magnitudes are much larger (~ 100 nA), making it more desirable for applications.

Fig. 1 shows a schematic of the device we consider. On the left and right end of the graphene sheet two external voltages $V_1(t) = V_1 + \delta V_1 \sin(\omega t)$ and $V_2(t) = V_2 + \delta V_2 \sin(\omega t + \phi)$ are applied. An external field $B_0\hat{z}$ is applied perpendicular to the graphene sheet in the central part of the sheet of length L , which forms the pumping region. Due to the finite width W of the sheet the transverse momenta are quantized. We consider short and wide pumps ($W \gg L$) for which the microscopic details of the edges become insignificant [22]. With the boundary condition that the mass of the carriers goes to infinity at $y = 0$ and $y = W$, the transverse momenta are quantized as $q_m = \frac{m\pi}{2W}$, where $m = 1, 3, 5, \dots$, with m labeling the modes [22]. Also, we assume that the dimensions of the pump are much larger than the carbon-

carbon lattice constant. In that case the intervalley tunneling is suppressed and it is sufficient to consider just one valley [23].

We use scattering matrix formalism for calculating the pumped current [3] and divide the system into three regions. In region 1 ($x < -L/2$) and region 3 ($x > L/2$) gate voltages $V_1(t)$ and $V_2(t)$ are applied, respectively. In these regions both up-spin and down-spin carriers obey the equation of motion described by the Hamiltonian $\mathcal{H} = v_F \sigma \cdot (\mathbf{p} + eV_j)$, where $j = 1$ for region 1 and $j = 2$ for region 3, \mathbf{p} is the momentum operator, v_F is the Fermi velocity and $\sigma = (\sigma_x, \sigma_y, \sigma_z)$ represents the three Pauli matrices. In region 2, we describe the effect of the magnetic field B_0 and include the effect of Zeeman splitting. We choose the Landau gauge, such that the vector potential is $\mathbf{A}(x) = (0, B_0 x, 0)$. Then in region 2 the Hamiltonian for up spin and down spin carriers is $\mathcal{H}_\uparrow = v_F \sigma \cdot (\mathbf{p} + e\mathbf{A}(x)) + g^* \mu_B B_0/2$ and $\mathcal{H}_\downarrow = v_F \sigma \cdot (\mathbf{p} + e\mathbf{A}(x)) - g^* \mu_B B_0/2$ respectively. Here g^* is the spin g-factor (assumed to be 2 [24]) of the carriers and μ_B represents the Bohr magneton. To simplify the notation we introduce dimensionless units: $l_B = \sqrt{\hbar/(eB_0)}$, $\mathbf{r} \rightarrow l_B \mathbf{r}$, $q_m \rightarrow q_m/l_B$, $k_x \rightarrow k_x/l_B$, $E \rightarrow E_0 E$, $E_0 = \hbar v_F/l_B$. k_x represents the momentum along the x -axis.

The pumped current into the left lead, in the adiabatic regime and for (bi)linear response, is given by [3]:

$$I_p = \frac{\omega e \sin \phi \delta V_1 \delta V_2}{2\pi} \sum_m \text{Im} \left[\frac{\partial r^*}{\partial V_1} \frac{\partial r}{\partial V_2} + \frac{\partial t^*}{\partial V_1} \frac{\partial t}{\partial V_2} \right]. \quad (1)$$

Here r and t represent the coefficients for reflection and transmission into the left reservoir and the index m sums over all the modes (a similar expression can be derived for pumping into the right reservoir). Note that we have different r and t for up-spin and down-spin. The pumped charge current is $I_p^{\text{charge}} = I_p^\uparrow + I_p^\downarrow$ and spin current is $I_p^{\text{spin}} = I_p^\uparrow - I_p^\downarrow$. To calculate r^\uparrow and t^\uparrow , we write down the wavefunctions in the three regions corresponding to the respective Hamiltonians, and then demand that the wavefunction is continuous across the boundaries at $x = -L/2$ and $x = L/2$. In region 1 the wavefunction is given by:

$$\Psi_1 = e^{iq_m y} \begin{pmatrix} e^{ik_x(x+L/2)} + r^\uparrow e^{-ik_x(x+L/2)} \\ e^{ik_x(x+L/2)} e^{i\phi_1} + r^\uparrow e^{-ik_x(x+L/2)} e^{-i\phi_1} \end{pmatrix}. \quad (2)$$

Here $\tan \phi_1 \equiv q_m/k_x$ and the energy of these excitations is given by $E = (eV_1 + \hbar v_F \sqrt{k_x^2 + q_m^2})/E_0$. Similarly, the wavefunction in region 3 is given by:

$$\Psi_3 = t^\uparrow e^{iq_m y} \begin{pmatrix} e^{ik'_x(x-L/2)} \\ e^{ik'_x(x-L/2)} e^{i\phi_2} \end{pmatrix}, \quad (3)$$

where $\tan \phi_2 \equiv q_m/k'_x$ and the energy of these excitations is given by $E = (eV_2 + \hbar v_F \sqrt{k_x'^2 + q_m^2})/E_0$. In the

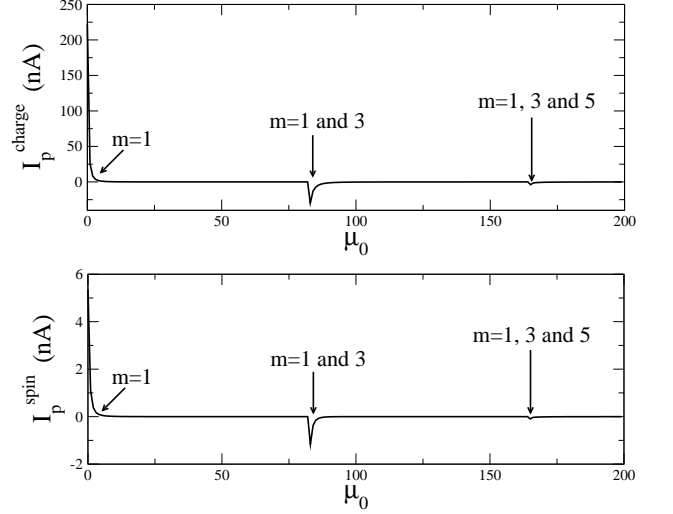


FIG. 2. Upper panel: pumped charge current as a function of μ_0 for $W = 5\mu\text{m}$, $L = 0.5\mu\text{m}$, $V_1 = V_2 = 0.1\text{ V}$, $\delta V_1 = \delta V_2 = 0.1\text{ mV}$, $\omega/(2\pi) = 5\text{ GHz}$ and $B_0 = 0.1\text{ T}$. Lower panel: same as the upper panel for the pumped spin current. See the text for more explanation.

central region the wavefunction can be written as a linear combination of Weber functions [25],

$$\Psi_2 = e^{iq_m y} \begin{pmatrix} C_1 D_{p-1}(z) + C_2 D_{p-1}(-z) \\ \frac{i\sqrt{2}}{E} [C_1 D_p(z) - C_2 D_p(-z)] \end{pmatrix}, \quad (4)$$

where $z = \sqrt{2}(x + q_m)$ and $p = (E - \frac{g^* \mu_B B_0}{2E_0})^2/2$. Setting $\alpha_3 = D_{p-1}(\sqrt{2}(q_m - L/2))$, $\alpha_4 = D_{p-1}(\sqrt{2}(-q_m + L/2))$, $\gamma_1 = \frac{\sqrt{2}}{E} D_p(\sqrt{2}(q_m - L/2))$, $\gamma_2 = \frac{\sqrt{2}}{E} D_p(\sqrt{2}(-q_m + L/2))$, $\omega_1 = D_{p-1}(\sqrt{2}(q_m + L/2))$, $\omega_2 = D_{p-1}(\sqrt{2}(-q_m - L/2))$, $\eta_1 = \frac{\sqrt{2}}{E} D_p(\sqrt{2}(q_m + L/2))$ and $\eta_2 = \frac{\sqrt{2}}{E} D_p(\sqrt{2}(-q_m - L/2))$, we find

$$t^\uparrow = \frac{2i(\eta_2 \omega_1 + \eta_1 \omega_2) \cos \phi_1}{f^+ g^+ - f^- g^-} \quad (5)$$

$$r^\uparrow = \frac{f^- h^+ - f^+ h^-}{f^+ g^+ - f^- g^-}, \quad (6)$$

where $f^+ = i\eta_2 + \omega_2 e^{i\phi_2}$, $f^- = i\eta_1 - \omega_1 e^{i\phi_2}$, $g^+ = i\gamma_1 + \alpha_3 e^{-i\phi_1}$, $g^- = i\gamma_2 - \alpha_4 e^{-i\phi_1}$, $h^+ = i\gamma_2 + \alpha_4 e^{i\phi_1}$ and $h^- = i\gamma_1 - \alpha_3 e^{i\phi_1}$. Similar expressions are found for r^\downarrow and t^\downarrow , the only difference being that $p = (E + \frac{g^* \mu_B B_0}{2E_0})^2/2$ instead of $p = (E - \frac{g^* \mu_B B_0}{2E_0})^2/2$. Note that due to broken time reversal symmetry the upward traveling (with prefactor $e^{iq_m y}$) and downward traveling (with prefactor $e^{-iq_m y}$) waves have different reflection and transmission coefficients.

Now we present the numerical results for the pumped charge and spin currents obtained using the above expressions for the reflection and transmission coefficients. The

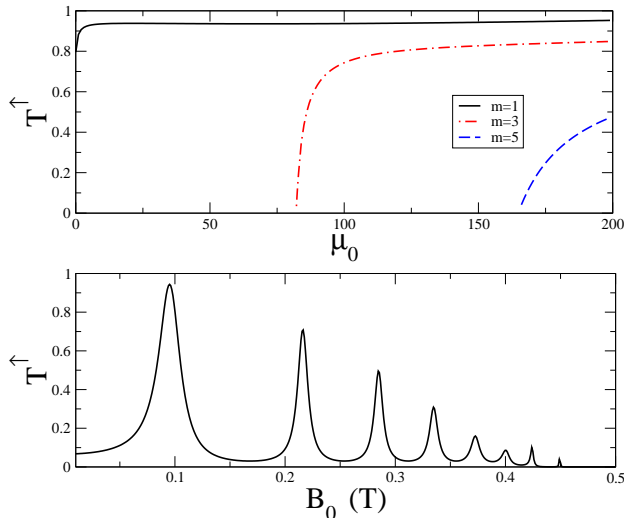


FIG. 3. (color online). Upper panel: transmission probability $T^\uparrow = t^{\uparrow*}t^\uparrow$ calculated for the up-spin carriers for the lowest modes as a function of μ_0 , for the same parameters as in Fig. 2. The solid line represents $m = 1$, the dot-dashed line represents $m = 3$ and the dashed line represents $m = 5$. Lower panel: transmission probability for the up-spin carriers as a function of external field B_0 . See the text for further explanation.

current is calculated using Eq. (1). We choose $W = 5\mu\text{m}$, $L = 0.5\mu\text{m}$, $V_1 = V_2 = 0.1\text{ V}$, $\delta V_1 = \delta V_2 = 0.1\text{ mV}$, $v_F = 10^6\text{ m/s}$ and $\omega/(2\pi) = 5\text{ GHz}$. [20, 24]. The phase difference between the two external voltages ϕ is chosen to be $\pi/2$ so as to maximize the pumped current. First we calculate the pumped current for fixed energy $E = \mu = 100.21\text{ meV} + 0.005\mu_0\text{ meV}$. μ represents the Fermi energy in the two leads and the single particle state energy in the central pumping region. All these energies are taken to be equal in order to eliminate the possibility of generating currents by an applied external bias and secure energy-conserved tunneling. Also the temperature is set to zero in all our calculations. The lowest energy of the carriers in the reservoirs with $k_x = 0$ and $m = 1$ is given by $eV_1 + \hbar v_F \frac{\pi}{2W}$ which is equal to 100.207 meV for the above mentioned parameters. μ is chosen to be $100.21\text{ meV} + 0.005\mu_0\text{ meV}$ in order to include the contribution of these lowest lying excitations. Fig. 2 shows the dependence of the pumped charge current (top panel) and spin current (bottom panel) on μ_0 for $B_0 = 0.1\text{ T}$. For $\mu_0 = 0$, only the lowest modes $m = 1$ contribute. As μ_0 increases higher modes $m = 3$ also start contributing which results in the peak around $\mu_0 = 82$ and similarly there is a peak when $m = 5$ starts contributing (around $\mu_0 = 164$). The above is true for both charge and spin currents. The top panel of Fig. 3 shows the transmission probability $T^\uparrow = t^{\uparrow*}t^\uparrow$ for $m = 1, 3$ and 5 . We also calcu-

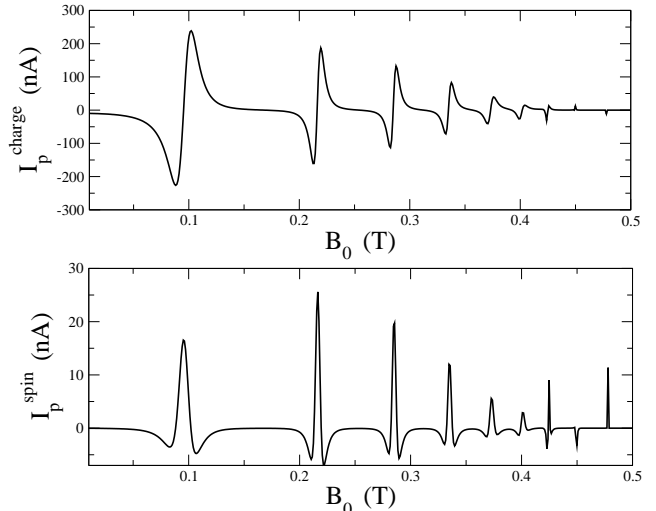


FIG. 4. Upper panel: pumped charge current for the same parameters as in Fig. 2 and $\mu_0 = 0$ as a function of B_0 . Lower panel: same as the upper panel for the pumped spin current. See the text for further explanation.

lated the transmission probability for down-spin carriers (not shown in Fig. 3) and it is almost identical to the one for up-spin carriers. While the transmission probability and hence the conductance $G \sim \text{Tr } T$, for all modes shown always *increases* with μ_0 , the pumped current initially *decreases* with μ_0 and then changes sign. This feature can be used to distinguish between any rectification current and the pumped current.

The upper panel of Fig. 4 shows the pumped charge current as we change the magnetic field at fixed chemical potential $\mu = 100.21\text{ meV}$, all other parameters being the same as in Fig. 2. The magnetic field is varied from 0.01 T to 0.5 T . As expected, the pumped currents are very sensitive to the magnetic field. The pumped current is large when the magnetic length l_B is comparable to the dimensions of the pump. For $B_0 = 0.1\text{ T}$, $l_B \sim 100\text{ nm}$ and we see large values of the pumped currents ($\sim 200\text{ nA}$) for the charge current. To understand this behavior and compare it to the conductance we calculate the transmission probability as a function of magnetic field for the same parameters, see the lower panel of Fig. 3. As before, the transmission probability for down-spin carriers (not shown) is almost identical. Each peak of the transmission probability corresponds to a large jump in pumped currents, and the pumped charge current changes sign around that peak. As we increase the magnetic field, the magnetic length decreases and becomes much smaller than the dimensions of the pump. Both the conductance and the pumped charge current *decreases* with increasing magnetic field. The lower panel of Fig. 4 shows the calculated spin current

for the same parameters. The peaks in the pumped spin current correspond to the peaks in the transmission probability. In general the pumped spin current is one order of magnitude smaller than the pumped charge current.

Finally, we comment on the experimental realization of this pump. Fabricating metallic gates on graphene nanostructures with widths ranging from 10-100 nm and lengths of 1-2 μm can be achieved using current technologies [9, 16]. Perhaps the most difficult part will be to apply local magnetic fields of strengths up to 0.5 T in the central pumping region. Many efforts have been made in this direction, for example using nanomagnets [26]. The latter can in principle be embedded under the central pumping region of the graphene pump. It should be noted that Eq. (1) represents the current pumped throughout one whole pumping cycle with no external bias applied. In practice because of the phase difference ϕ between $V_1(t)$ and $V_2(t)$ (chosen to be $\pi/2$), there will be a small bias across the pump. The pump cycle can be chosen in a symmetric way such that the bias reverses after half of the period and any rectification current over the whole cycle is canceled.

To summarize, we have proposed a quantum pump based on graphene in a perpendicular magnetic field. The pumped current is carried by traveling modes and has a large magnitude (~ 100 nA). We find that the pumped current has a characteristic dependence on B_0 . Experimental verification of the pump properties will provide a much needed demonstration of the phenomenon of quantum pumping.

This research was supported by the Dutch Science Foundation NWO/FOM.

[1] M. Büttiker, H. Thomas, and A. Prêtre, *Z. Phys. B* **94**, 133 (1994).
 [2] B. Spivak, F. Zhou, and M. T. Beal Monod, *Phys. Rev. B* **51**, 13226 (1995).
 [3] P. W. Brouwer, *Phys. Rev. B* **58** 10135(R) (1998).
 [4] B. L. Altshuler, and L. I. Glazman, *Science* **283** 1864 (1999).
 [5] E. R. Mucciolo, C. Chamon, and C. M. Marcus, *Phys. Rev. Lett.* **89**, 146802 (2002).
 [6] M. Switkes, C. M. Marcus, K. Campman, and A. D. Gos-

sard, *Science* **283**, 1905 (1999).
 [7] S. K. Watson, R. M. Potok, C. M. Marcus, and V. Umansky, *Phys. Rev. Lett.* **91**, 258301 (2003).
 [8] P. W. Brouwer, *Phys. Rev. B* **63**, 121303(R) (2001).
 [9] Y. Zhang, J.-W. Tan, H. L. Stormer and P. Kim, *Nature (London)* **438**, 201 (2005).
 [10] K. S. Novoselov, A. K. Geim, S. V. Morozov, D. Jiang, M. I. Katsnelson, I. V. Grigorieva, S. V. Dubonos and A. A. Firsov, *Nature (London)* **438**, 197 (2005).
 [11] A. H. Castro Neto, F. Guinea, N. M. R. Peres, K. S. Novoselov, and A. K. Geim, *Rev. Mod. Phys.* **81**, 109 (2009).
 [12] C. Berger, Z. Song, X. Li, X. Wu, N. Brown, C. Naud, D. Mayou, T. Li, J. Hass, A. N. Marchenkov, E. H. Conrad, P. N. First, W. A. de Heer, *Science* **312**, 1191 (2006).
 [13] A. K. Geim and K. S. Novoselov, *Nature Mater.* **6**, 183 (2007).
 [14] V. S. Novoselev, A. K. Geim, S. V. Morozov, D. Jiang, M. I. Katsnelson, I. V. Grigorieva, S. V. Dubonos and A. A. Firsov, *Nature* **438**, 197 (2005).
 [15] M. S. Purewal, Y. Zhang, and P. Kim, *Phys. Stat. Solidi B* **243**, 4318 (2006).
 [16] M. Y. Han, B. Özyilmaz, Y. Zhang, and P. Kim, *Phys. Rev. Lett.* **98**, 206805 (2007).
 [17] E. W. Hill, A. K. Geim, K. S. Novoselev, F. Schedin, and P. Blake, *IEEE Trans. Magn.* **42**, 2694 (2008).
 [18] S. Cho and M. S. Fuhrer, *Phys. Rev. B* **77**, 081402(R) (2008).
 [19] R. P. Tiwari and D. Stroud, *Phys. Rev. B* **79**, 165408 (2009).
 [20] R. Zhu and H. Chen, *Appl. Phys. Lett.* **95**, 122111 (2009).
 [21] E. Prada, P. San-Jose, and H. Schomerus, *Phys. Rev. B* **80**, 245414 (2009).
 [22] J. Tworzydło, B. Trauzettel, M. Titov, A. Rycerz, and C. W. J. Beenakker, *Phys. Rev. Lett.* **96**, 246802 (2006) (arXiv:cond-mat/0603315v3).
 [23] T. Ando and T. Nakanishi, *J. Phys. Soc. Jpn.* **67**, 1704 (1998).
 [24] Y. Zhang, Z. Jiang, J. P. Small, M. S. Purewal, Y.-W. Tan, M. Fazlollahi, J. D. Chudow, J. A. Jaszczak, H. L. Stormer, and P. Kim, *Phys. Rev. Lett.* **96**, 136806 (2006).
 [25] M. Ramezani Masir, P. Vasilopoulos, A. Matulis, and F. M. Peeters, *Phys. Rev. B* **77**, 235443 (2008).
 [26] V. Kubrak, A. Neumann, B. L. Gallagher, P. C. Main, M. Henini, C. H. Marrows, and B. J. Hickey, *J. Appl. Phys.* **87**, 5986 (2000); K. S. Novoselov, A. K. Geim, S. V. Dubonos, Y. G. Cornelissens, F. M. Peeters, and J. C. Maan, *Physica E* **12**, 244 (2002); M. Pioro-Ladrière, T. Obata, Y. Tokura, Y.-S. Shin, T. Kubo, K. Yoshida, T. Taniyama, and S. Tarucha, *Nature Phys.* **4**, 776 (2008).